

Learning to Trace and Untangle Semi-planar Knots (TUSK)

Vainavi Viswanath^{*1}, Kaushik Shivakumar^{*1}, Jainil Ajmera¹, Mallika Parulekar¹, Justin Kerr¹, Jeffrey Ichnowski¹, Richard Cheng², Thomas Kollar², Ken Goldberg¹

Abstract—This paper extends prior work on untangling long cables and presents TUSK (Tracing to Untangle Semi-planar Knots), a learned cable-tracing algorithm that resolves overcrossings and undercrossings to recognize the structure of knots and grasp points for untangling from a single RGB image. This work focuses on semi-planar knots, which are knots composed of crossings that each include at most 2 cable segments. We conduct experiments on long cables (3 m in length) with up to 15 semi-planar crossings across 6 different knot types. Crops of crossings from 3 knots (overhand, figure 8, and bowline) of the 6 are seen during training, but none of the full knots are seen during training. This is an improvement from prior work on long cables that can only untangle 2 knot types. Experiments find that in settings with multiple identical cables, TUSK can trace a single cable with 81% accuracy on 7 new knot types. In single-cable images, TUSK can trace and identify the correct knot with 77% success on 3 new knot types. We incorporate TUSK into a bimanual robot system and find that it successfully untangles 64% of cable configurations, including those with new knots unseen during training, across 3 levels of difficulty. Supplementary material, including an annotated dataset of 500 RGB-D images of a knotted cable along with ground-truth traces, can be found at <https://sites.google.com/view/tusk-rss>.

I. INTRODUCTION

In industrial and household settings, tangled long cables can pose a threat to the safety of individuals, especially older or at-risk adults, by impeding their movement. Additionally, in environments where heavy machinery is operated, cables can get caught in moving parts and cause potential damage or harm [27, 21, 37, 43].

Untangling long cables can be difficult due to challenges in manipulation and perception alike. Developing manipulation primitives that can adapt to different knot topologies is non-trivial since knot dynamics are challenging to predict and can depend on unobservable parameters of the cable like stiffness. Also, estimating cable state from an RGB image is difficult since long cables often fall into complex configurations with many crossings. Long cables can also contain a significant amount of free cable (referred to as *slack*), which can occlude and inhibit the perception of true knots from an overhead image. The task of autonomously untangling cables requires a generalizable system that can track a cable path in complex configurations and handle the wide distribution of knots present in long cables.

Much of prior work bypasses full state estimation by employing object detection networks and keypoint selection

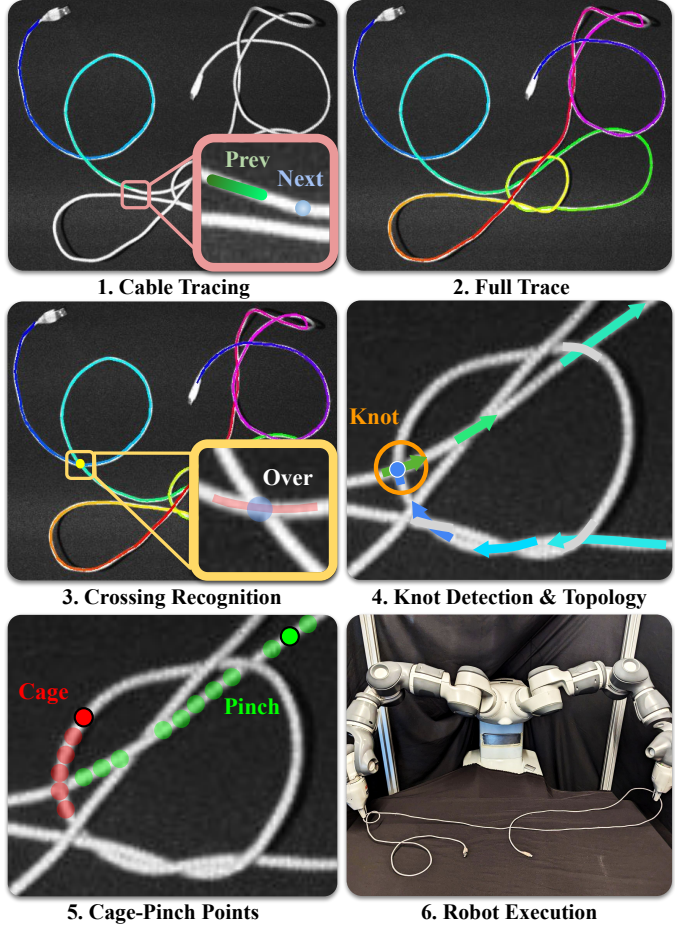


Fig. 1: TUSK: TUSK first performs cable tracing (1, 2). The trace is shown through a rainbow gradient (from violet to purple), depicting the sequence in which the cable is traced. After tracing, TUSK does crossing recognition (3) to obtain the full topology of the cable. Next, using crossing cancellation rules from knot theory, it analytically determines knots (4) in the cable. Next, TUSK surveys possible cage-pinch points (5) and selects the best candidate points to grasp to execute a cage-pinch dilation action, untangling the knot (6).

networks to identify knots and grasp points directly based on geometric patterns [39, 31]. These works can disentangle 2 types of knots (overhand and figure-8), but the methods do not generalize well to the large number of complex configurations long cables can form. Other prior work is able to achieve some generality for knot disentanglement, but only for short cables up to 15 cm in length. In such short cables, the knot configurations are less complex, and there is little difficulty with slack management, eliminating the need to estimate the cable path [38, 7, 34, 32]. This work considers long cables

^{*} Equal Contribution

¹ AUTOLAB at University of California, Berkeley

² Toyota Research Institute (TRI)

up to 3 meters in length consisting of semi-planar knots, i.e. knots comprised of semi-planar crossings, where each crossing consists of at most 2 cable segments when viewed from above. The single-cable semi-planar knots considered in this work are overhand, figure 8, overhand honda, bowline, linked overhand, and figure 8 honda knots. The double-cable semi-planar knots considered in this work are carrick bend, sheet bend, and square knots. This paper focuses on high-accuracy state estimation techniques and algorithms grounded in knot theory to process the results of state estimation and select untangling actions for a broader class of knots.

This paper presents TUSK, which makes the following contributions:

- 1) A novel cable state estimator consisting of a learning-based iterative tracer and a crossing classifier with a crossing correction algorithm.
- 2) An analytic knot detection algorithm and untangling point selection algorithm given the cable state estimates.
- 3) Data from physical experiments using TUSK to untangle semi-planar knots. Results suggest TUSK can correctly trace and segment a single cable in multi-cable settings with 81% accuracy, detect knots with 77% accuracy, and function in a physical system for untangling semi-planar knots with 64% untangling success in under 8 minutes.

II. RELATED WORK

A. Deformable Object Manipulation

Robot manipulation of deformable objects, such as cables (1D), fabric (2D), and bags (3D), is difficult because they have a near-infinite state space, can form self-occlusions, and are difficult to model. This study focuses on the problem of untangling knots in long cables. Recently, there has been progress in deformable manipulation, including algorithms for untangling cables [7, 34, 38, 19], smoothing and folding fabric [29, 41, 6, 8, 15, 36, 9], and placing objects into bags [30, 2].

Methods for intelligently and autonomously manipulating deformable objects lie on a spectrum ranging from completely model-free, directly perception-driven approaches to those that directly estimate the state of the object of interest and then perform planning on it.

Examples of model-based methods for deformable objects are dense descriptors [5], which have been applied to cable knot tying [33] and fabric smoothing [6], as well as visual dynamics models for non-knotted cables [44, 40] and fabric [8, 44, 17]. Model-free approaches include reinforcement or self-supervised learning for fabric smoothing and folding [20, 42, 16, 1] and straightening curved ropes [42], or directly imitating human actions [29].

B. Cable Perception, Manipulation, and Untangling

Pioneering research in untangling, such as that conducted by Lui and Saxena [18], relies on decomposing point clouds of rope into segments which are refined into a graphical representation of the cable’s structure based on priors on cable behavior such as bending radius. Other methods learn

visual models for cable manipulation over which to plan [23], investigate iteratively refining dynamic actions [3], or use approximate state dynamics along with a learned error function [22]. Fusing point clouds across time has shown success in tracking segments of cable provided they are not tangled on themselves [28, 35].

Studies on dense knots, such as those by Grannen et al. [7] and Sundaresan et al. [34], employ learning-based keypoint detection to parameterize action primitives for untangling isolated knots. The work of Viswanath et al. [39] expands on this idea to long (3m) cables, with the addition of a learned knot detection pipeline. This approach works well for a certain range of knot types within the model’s training distribution as it uses end-to-end perception systems trained on human labels. Scaling these methods to arbitrary knot types would require an intractable amount of human labels, motivating the local topology estimation approach in this work.

Prior cable state estimation work includes that led by Huang et al. [10], which estimates the topological state of multiple ropes against varying backgrounds and uses primitives to untangle rope configurations consisting primarily of loops with 2 to 4 crossings. Additional linear deformable tracing work includes that of Keipour et al. [13], which models cables as chains of jointed cylindrical bodies, then uses the model for routing tasks. The works of Jackson et al. [12] and Padoy and Hager [24] trace surgical strings in stereo or mono images by optimizing a continuous spline representation. In contrast, this work primarily focuses on much longer cables with a greater variety of configurations, for which analytical methods struggle to differentiate nearby, twisted cables. Some prior work approaches this problem [25] but does not fully estimate cable state, only identifying crossings.

III. PROBLEM STATEMENT

The objective is to bring a long (3 m) cable containing semi-planar knots into an untangled configuration, where no knots remain (knots defined in Section III-A).

The workspace is defined by an (x, y, z) coordinate system and consists of a bilateral robot and a foam-padded manipulation surface, which lies in the (x, y) plane. The workspace also contains a fixed overhead RGB-D camera that faces the manipulation surface and outputs grayscale images and depth data. However, depth data is not used in TUSK. Rather, it is only used during manipulation. We work with a 300 cm cable. We assume the cable is visually distinguishable from the manipulation surface, its initial configuration has at least one endpoint visible, and is semi-planar as assumed in Grannen et al. [7], meaning each crossing in the knot has at most 2 intersecting cable segments. For perception experiments, we work with knots as tight as 5 cm in diameter. For physical experiments, due to robot graspability constraints, we work with knots of varying density, or approximate diameter, upwards of 10 cm in diameter. We define cable state to be $\theta(s) = \{(x(s), y(s), z(s))\}$ where s is an arc-length parameter that ranges $[0, 1]$, representing the normalized length of the cable. Here, $(x(s), y(s), z(s))$ is the location of a cable point

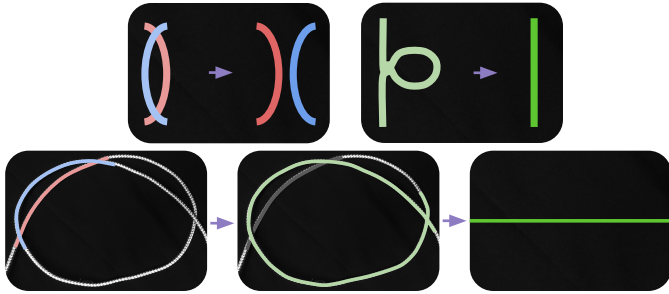


Fig. 2: **Reidemeister Moves and Crossing Cancellation:** Top left depicts Reidemeister Move II. Top right depicts Reidemeister Move I. The bottom row shows that by algorithmically applying Reidemeister Moves II and I, we can cancel trivial loops, even if they visually appear as knots.

at a normalized arc length of s from the cable’s first endpoint. We also define the range of $\theta(s)$ —that is, the set of all points on the cable at time t —to be \mathcal{C}_t .

A. Knot Definition

Consider a pair of points p_1 and p_2 on the cable path at time t with $(p_1, p_2 \in \mathcal{C}_t)$. Knot theory strictly operates with closed loops, so to form a loop with the current setup, we construct an imaginary cable segment with no crossings joining p_1 to p_2 [26]. This imaginary cable segment passes above the manipulation surface to complete the loop between p_1 and p_2 (“ $p_1 \rightarrow p_2$ loop”). A knot exists between p_1 and p_2 at time t if no combination of Reidemeister moves I, II (both shown in Figure 2), and III can simplify the $p_1 \rightarrow p_2$ loop to an unknot, i.e. a crossing-free loop. In this paper, we aim to untangle semi-planar knots. For convenience, we define an indicator function $k(s) : [0, 1] \rightarrow \{0, 1\}$ which is 1 if the point $\theta(s)$ lies between any such points p_1 and p_2 , and 0 otherwise.

Based on the above knot definition, this objective is to remove all knots, such that $\int k(s)_0^1 = 0$. In other words, the cable, if treated as a closed loop from the endpoints, can be deformed into an unknot. We measure the success rate of the system at removing knots, as well as the time taken to remove these knots.

IV. METHODS

We present TUSK (Tracing to Untangle Semi-planar Knots) a system that takes grayscale images as input and reconstructs the state of a cable with semi-planar knots and crossings, performs knot detection, and selects graspable points for untangling. The first component is an iterative, learned cable tracer which estimates the path the cable takes through an image observation, combined with a crossing classifier which classifies over and under-crossings. Together, these estimate the state of the cable. TUSK then analyzes the state to detect knots and find graspable points for untangling. We will reference these points as *cage-pinch points* since during manipulation, one of these points receives a pinch grasp and the other a cage grasp (Section V).

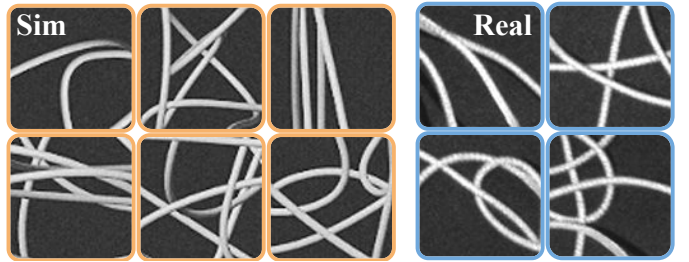


Fig. 3: **Simulated and real crops used for training TUSK:** On the left are simulated cable crops augmented with Gaussian noise, brightness, and sharpening to match the real images (right) as closely as possible.

A. Learned Cable Tracer

We frame the problem of tracing a cable as estimating the most likely sequence of points that the cable passes through, where the goal of each step is to produce a probability distribution over the next point given the past points. This module estimates the spline (“trace”) of the cable in an image by sequentially performing inference using a neural network on image crops. At each step, the model takes in a crop of the image along with trace points from previous iterations and predicts a heatmap, where we interpret the argmax as the next point along the trace. Since it operates on crops, the model suffers less from overfitting and benefits from more easy sim-to-real transfer as it operates on local information about the cable, rather than global visual and geometric appearance of knots.

1) *Initialization:* To initialize the trace, we supply a start pixel along the cable (in practice, one endpoint). We use an analytic tracer as in [31] to trace approximately 96 pixels, then use these points to initialize the learned tracer, as the model requires previous trace points to predict the next point along the trace.

2) *Model Architecture and Inference:* After initialization, the tracer sequentially applies a learned model to grow the trace. At each step, the network receives an input of an overhead image cropped to the center of the last predicted trace point, 64×64 pixels. To provide the model with information about the cable’s previous path, we fuse the previous points of the trace into a gradient segmented line with the same thickness as the cable. The most recently traced point is brightest and the line decreases in brightness until it exits the crop. This is included in one channel of the input image. The other two channels contain an identical version of the grayscale image. The input dimension to the model is thus $64 \times 64 \times 3$. The model outputs a $64 \times 64 \times 1$ heatmap indicating the likelihood of each pixel being the next step in the cable trace. We choose the highest point in this heatmap as the next point in the trace. This process is applied iteratively until the tracer reaches another endpoint or leaves the visible workspace.

We use the UNet architecture for the model, which is known to be effective in image segmentation tasks [11]. Section IV-A3 describes the dataset and training process. Each point in the trace is approximately 12 pixels apart, chosen by grid search to provide a balance between adding context and reducing

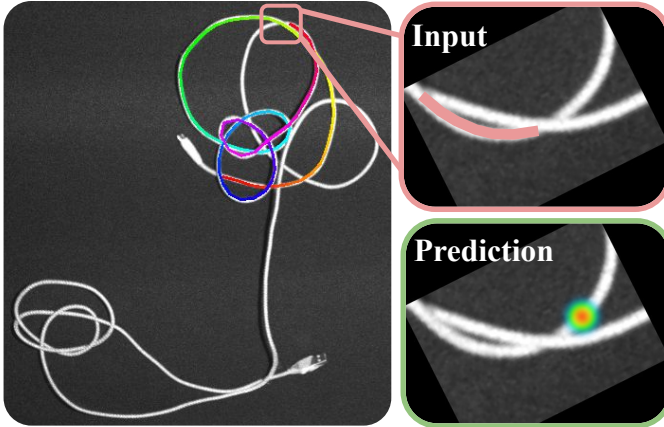


Fig. 4: **Input and Prediction of Iterative Learned Cable Tracer:** the iterative learned cable tracer takes small crops around the cable and one step at a time, predicts the next point in the trace. The input crop is a $64 \times 64 \times 3$ crop centered on the previous trace point. The first channel contains the previous trace points within the crop. The second and third channel are the gray scale image of the crop. The prediction is a 64×64 heatmap, where we infer the argmax of the heatmap to be the next point in the trace.

overfitting. To reduce the input space for the model and thus increase data efficiency, we pre-rotate the input image such that the last two points of the trace are aligned horizontally and the trace always travels left to right with the most recently traced point being the right most point. We explore another important tradeoff between context and overfitting via grid search by tuning the size of the crop, 64×64 , and number of previous points inputted into the model, 3.

3) *Dataset and Model Training:* To train the Learned Tracer model, we leverage simulation to procedurally generate a dataset which encompasses a wide distribution of crossing configurations. Using Blender [4], we collect a dataset of 30,000 simulated grayscale images, whose visual appearance closely matches real observations (Fig. 3). Cable configurations are generated via random Bezier curves through the following 3 methods: (1) a weighted combination of successively choosing random points outside of a small exclusion radius around the current point, (2) segments intentionally designed to be near-parallel, and (3) other sections of cable designed to appear dense and knot-like by confining certain segments of the cable to regions in space.

We sample image crops randomly along the cable, with 95% of samples distributed on cable crossings, as these represent the challenging cases. The simulated images are augmented with Gaussian noise with standard deviation of 6, brightness with standard deviation of 5, and sharpening to imitate the appearance of real cable crops. Additionally, we augment the dataset with a smaller dataset of 568 real, grayscale cable crop images hand-labeled with splines, sampled during training such that real images are approximately 20% of the examples seen. During training we use the Adam optimizer [14] with pixelwise binary cross-entropy loss, using a batch size of 64 and learning rate of 10^{-5} .

B. Over/Undercrossing Predictor

To convert the 2D trace of a cable into a topology for the downstream task of untangling, we use a convolutional neural network (CNN) to classify over and under-crossings in the cable.

1) *Data and Model Input:* We use simulated and real over/undercrossing crops of size 20×20 . Similar to the cable tracer, the 568 real images are oversampled such that they are seen 20% of the time during training. The simulated data is augmented in the same manner to the cable tracer to imitate the appearance of real cable crossings when observed as 20×20 crops. We provide the network with a $20 \times 20 \times 3$ crop as input. The first channel encodes the points of the trace indicating the cable segment of interest (in other words, the cable segment with respect to which we aim to classify the crossing as an over/undercrossing). Similar to how the points are inputted for the learned tracer, the points are fused together into a line segment, but now the line segment does not decrease in brightness as points become less recent. The crop is rotated so the first and last point in the line segment are horizontal. The second channel is a Gaussian heatmap centered at the position of the crossing we aim to classify. This helps deal with dense configurations that can have nearby consecutive crossings captured in the same crop. By receiving a position of interest, the network learns to ignore other crossings. Lastly, as all images are grayscale, the third channel encodes the grayscale image of the cable crossing.

2) *Model Architecture and Inference:* We use a ResNet-34 classification model to output a prediction score in the interval $[0, 1]$. This model is trained using binary cross-entropy loss with a single output unit with sigmoid activation. We tune a threshold to binarize the output by determining accuracy on a held-out validation set of 75 images on threshold values in the range $[0.05, 0.95]$ at intervals of 0.05. Based on the tuning results, we obtain a threshold of 0.275 such that a prediction score < 0.275 corresponds to an undercrossing prediction and a score ≥ 0.275 corresponds to an overcrossing prediction. We output the raw prediction score along with a scaled confidence value (ranging $[0.5, 1]$) indicating the probability associated with the classifier's prediction.

C. Analytic Knot Detection

We construct line segments between consecutive points on the trace outputted by the learned cable tracer (Section IV-A). Crossings are located at the points of intersection of these line segments. We use the crossing classifier (Section IV-B) to estimate whether these crossings are over/undercrossings. We also implement probabilistic crossing correction with the aim of rectifying classification errors, as we describe in Section IV-C1.

We denote the sequence of corrected crossings, in the order that they are encountered in the trace, by $\mathcal{X} = (c_1, \dots, c_n)$, where n is the total number of crossings and c_1, \dots, c_n represent the crossings along the trace. To reduce the number of actions required to successfully untangle the cable, we algorithmically apply Reidemeister moves I and II to discard

non-essential crossings (Fig. 2). We exclude Reidemeister move III from this scheme as it does not lead to a direct reduction in the number of crossings, unlike moves I and II. We are allowed to perform this algorithmic manipulation as Reidemeister moves maintain knot equivalence [26].

1) *Crossing Correction*: Given the assumption of knot semi-planarity, a single crossing location must contain one overcrossing and one undercrossing. In situations where the over/undercrossing classifier incorrectly predicts that the crossings at a location are both overcrossings or both undercrossings, we defer to the detection with higher confidence to correct the crossing assignment. The algorithm updates the probability associated with the corrected crossing to 1— its original value. This is to take into account model uncertainty when calculating confidence scores for the overall knot.

2) *Crossing Cancellation*: Crossing cancellation allows for the simplification of cable structure by removing non-essential crossings, shown in Figure 2. It allows the system to filter out some trivial configurations. We cancel all pairs of consecutive crossings (c_i, c_{i+1}) in \mathcal{X} for some j) that meet any of the following conditions:

- *Reidemeister I*: c_i and c_{i+1} are at the same location, or
- *Reidemeister II*: c_i and c_{i+1} are at the same set of locations as c_j and c_{j+1} ($c_j, c_{j+1} \in \mathcal{X}$). Additionally, c_i and c_{i+1} are either both overcrossings or both undercrossings.

We also cancel (c_j, c_{j+1}) in this case.

We algorithmically perform alternating Reidemeister moves I and II as described. We iteratively apply this step on the subsequence obtained until there are no such pairs left. We denote the final subsequence, where no more crossings can be canceled, by \mathcal{X}' .

3) *Knot Detection*: We say that a subsequence of \mathcal{X}' , $\mathcal{K}_{ij} = (c_i, \dots, c_j)$, defines a potential knot if:

- c_i is an undercrossing, and
- c_j is an overcrossing at the same location, and
- at least one intermediate crossing, i.e. crossing in \mathcal{X}' that is not c_i or c_j , is an overcrossing.

The first invariant is a result of the fact that all overcrossings preceding the first undercrossing (as seen from an endpoint) are removable. We can derive this by connecting both endpoints from above via an imaginary cable (as in Section III-A): all such overcrossings can be removed by manipulating the loop formed. The second invariant results from the fact that a cable cannot be knotted without a closed loop of crossings. The third and final invariant can be obtained by noting that a configuration where all intermediate crossings are undercrossings reduces to the unknot via the application of the 3 Reidemeister moves. Therefore, for a knot to exist, it must have at least one intermediate overcrossing.

Notably, these conditions are necessary, but not sufficient, to identify knots. However, they improve the likelihood of bypassing trivial configurations and detecting knots. This increases the system’s efficiency by enabling it to focus its actions on potential knots.

D. Algorithmic Cage-Pinch Point Detection

As per the definition introduced in Section IV-C3, given knot $\mathcal{K}_{ij} = (c_i, \dots, c_j)$, c_i and c_j define the segments that encompass the knot where c_i is an undercrossing and c_j is an overcrossing for the same crossing. The pinch point is located on the overcrossing cable segment, intended to increase space for the section of cable and endpoint being pulled through. The cage point is located on the undercrossing cable segment. To determine the pinch point, we search from crossing c_{u1} to crossing c_{u2} . c_{u1} is the previous undercrossing in the knot closest in the trace to j . $u2 > j$ and c_{u2} is the next undercrossing after the knot. We search in this region and select the most graspable region to pinch at, where graspability (G) is defined by the number of pixels that correspond to a cable within a given crop and a requirement of sufficient distance from all crossings c_i . To determine the cage point, we search from crossing c_i to c_k where $i < k < j$ and c_k is the next undercrossing in the knot closest in the trace to c_i . We similarly select the most graspable point. If no points in the search space for either the cage or pinch point are graspable, meaning $G < \mathcal{T}$ where \mathcal{T} is an experimentally derived threshold value, we continue to step along the trace from c_{u2} for pinch and from c_k for cage until $G \geq \mathcal{T}$. This search process is shown in Figure 1.

V. ROBOT UNTANGLING USING TUSK

A. Manipulation Primitives

We use the same primitives as in SGTM 2.0 (Sliding and Grasping for Tangle Manipulation 2.0) [31] to implement TUSK as shown in Figure 5 for untangling long cables. We add a *perturbation* move.

1) *Cage-Pinch Dilation*: We use cage-pinch grippers as in Viswanath et al. [39]. We have one gripper cage grasp the cable, allowing the cable to slide between the gripper fingers but not slip out. The other gripper pinch grasps the cable, holding the cable firmly in place. This is crucial for preventing knots in series from colliding and tightening during untangling. The *partial* version of this move introduced by Shivakumar et al. [31] separates the grippers to a small, fixed distance of 5 cm.

2) *Reveal Moves*: First, we detect endpoints using a Mask R-CNN object detection model. If both endpoints are visible, the robot performs an *Endpoint Separation Move* by grasping at the two endpoints and then pulling them apart and upwards, away from the workspace, allowing gravity to help remove loops before placing the cable back on the workspace. If both endpoints are not visible, the robot performs an *Exposure Move*. This is when it pulls in cable segments exiting the workspace. Building on prior work, we add a focus on where this move is applied. While tracing, if we detect the trace hits the edge, we perform an exposure move at the point where the trace exits the image.

3) *Perturbation Move*: If an endpoint or the cable segment near an endpoint has distracting cable segments nearby, making it difficult for the analytic tracer to trace, we perturb it

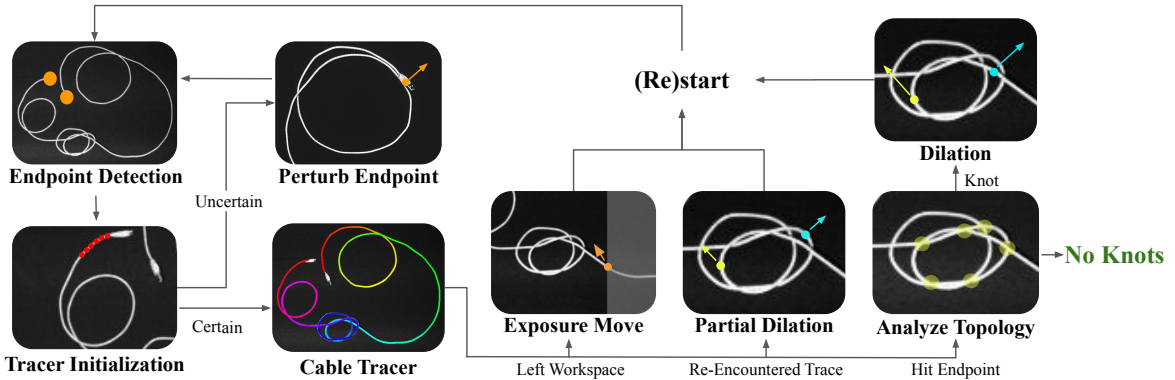


Fig. 5: **Untangling Algorithm with TUSK:** We first detect the endpoints and initialize the tracer with start points. If we are not able to obtain start points, we perturb the endpoint and try again. Next, we trace. While tracing, if the cable exits the workspace, we pull the cable towards the center of the workspace. If the tracer gets confused and begins retracing a knot region, we perform a partial cage-pinch dilation that will loosen the knot, intended to make the configuration easier to trace on the next iteration. If the trace is able to successfully complete, we analyze the topology. If there are no knots, we are done. If there are knots, we perform a cage-pinch dilation and return to the first step.

by grasping it and translating in the x-y plane by uniformly random displacement in a $10\text{cm} \times 10\text{cm}$ square in order to separate it from slack.

B. Cable Untangling System

Combining TUSK and the manipulation primitives from Section V-A, the cable untangling algorithm works as follows: First, detect endpoints and initialize the learned tracer with 6 steps of the analytic tracer. If TUSK is unable to get these initialization points, perturb the endpoint from which we are tracing and return to the endpoint detect step. Otherwise, during tracing, if the cable leaves the workspace, perform an exposure move. If the trace fails and begins retracing itself, which can happen in denser knots, perform a partial cage-pinch dilation as in [31]. If the trace completes and reaches the other endpoint, analyze the topology. If knots are present, determine the cage-pinch points for it, apply a cage-pinch dilation move to them, and repeat the pipeline. If no knots are present, the cable is considered to be untangled. The entire system is depicted in Figure 5.

VI. EXPERIMENTS

We test the performance of 1) TUSK, 2) the learned cable tracer, and 3) TUSK applied to autonomous robot untangling.

A. Workspace

The workspace consists of a $1\text{m} \times 0.75\text{m}$ surface with a bimanual ABB YuMi robot and an overhead Photoneo PhoXi camera with $773 \times 1032 \times 4$ RGB-D observations. Although there are 3 color channels, images outputted by the PhoXi are grayscale. Additionally, the workspace is padded with a 5 cm tall piece of foam and covered with a black cloth.

B. TUSK Setup

To test TUSK, we use a single 3 m, white, braided USB-A to micro-USB cable to the workspace.

We test TUSK on 3 different categories of cable configurations, shown in Figure 6. The ordering of the categories for these experiments does not indicate varying difficulty. Rather, they are 3 categories of knot configurations to test TUSK on.

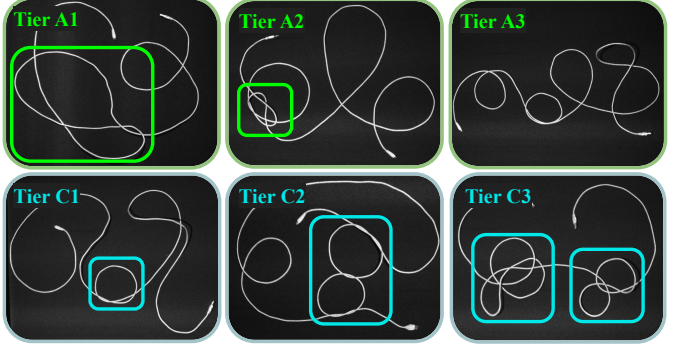


Fig. 6: Starting configurations for the 3 categories for TUSK experiments and the 3 levels for physical experiments.

- 1) **Tier A1:** Loose (35-40 cm in diameter) figure 8, overhand, overhand honda, bowline, linked overhand, and figure 8 honda knots.
- 2) **Tier A2:** Dense (5-10 cm in diameter) figure 8, overhand, overhand honda, bowline, linked overhand, and figure 8 honda knots.
- 3) **Tier A3:** Fake knots (trivial configurations positioned to appear knot-like from afar).

We evaluate TUSK on the 3 categories across the following ablations:

- 1) SGTM 2.0 perception system: using a Mask R-CNN model trained on overhand and figure-8 knots for knot detection.
- 2) TUSK (-LT): replacing the Learned Tracer with the same analytic tracer from Shivakumar et al. [31] as described in Section VI-C combined with the topology identification and knot detection methods without learned tracing.
- 3) TUSK (-CC): using the learned tracer and topology identification scheme to do knot detection without Crossing Cancellation, the iterative algorithmic application of Reidemeister moves I and II.
- 4) TUSK: the full perception system.

We report the success rate of each of these algorithms in the following manner. If a knot is present, the algorithm is successful if it correctly detects the first knot and correctly labels the first undercrossing corresponding to that knot. If

there are no knots, the algorithm is successful if it correctly detects no knots.

C. Tracing in Multi-Cable Settings Setup

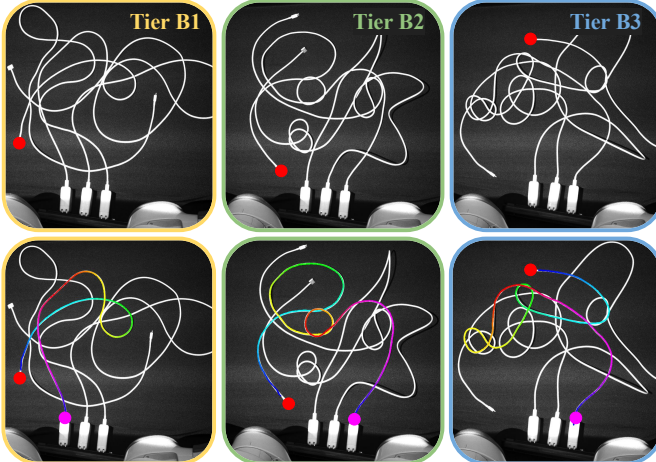


Fig. 7: Multi-cable tracing: **Top row:** illustrative examples of each of the 3 tiers of difficulty for multi-cable tracing experiments. **Bottom row:** Corresponding successful traces outputted by the learned tracer.

For this set of perception experiments, the workspace contains a power strip. Attached to the power strip are 3 MacBook adapters, with two 3m USB-C to USB-C cables and one 2m plain white USB-C to MagSafe 3 cable. This setup is depicted in the top row of Figure 7. We evaluate perception on multi-cable settings on 3 tiers of difficulty.

- 1) **Tier B1:** No knots; cables are dropped onto the workspace, one at a time.
- 2) **Tier B2:** Each cable is tied with a single knot that is 5-10 cm in diameter (one of figure 8, overhand, overhand honda, bowline, linked overhand, and figure 8 honda). The cables are then randomly dropped onto the workspace, one after another.
- 3) **Tier B3:** Each cable is tied with another cable through the following 2 cable knot types (square, carrick bend, and sheet bend) with up to 3 knots in the scene. As in the other tiers, the cables are randomly dropped onto the workspace, one by one.

Across all 3 tiers, we assume the cable of interest cannot exit and re-enter the workspace and that crossings must be semi-planar. Additionally, we pass in the locations of all 3 adapters to the tracer and an endpoint to initialize from. To account for noise in the input images, we take 3 images of each configuration and count the experiment a success if 2/3 have the correct trace and reach their corresponding adapter, otherwise we report a failure.

We evaluate the performance of the learned tracer from TUSK against an analytic tracer from Shivakumar et al. [31] as a baseline with scoring rules inspired by the work of Lui and Saxena [19] and Keipour et al. [13]. The analytic tracer explores all potential paths and determines the most correct trace through a scoring metric from [31]. The scoring metric prefers paths that reach an endpoint, discarding traces that do not reach adapters. This is because the scoring metric sees

TABLE I: TUSK Experiments

	SGTM 2.0	TUSK (-LT)	TUSK (-CC)	TUSK
Tier A1	2/30	14/30	20/30	24/30
Tier A2	28/30	8/30	21/30	26/30
Tier A3	12/30	14/30	0/30	19/30
Failures	(A) 30, (B) 18	(D) 11, (F) 7 (G) 24, (H) 11	(B) 38, (C) 5, (E) 6	(B) 11, (D) 8 (F) 1

reaching an endpoint as indicative of completing a trace. Of the paths that reach an endpoint, the trace returned is the one with the least sharp angle deviations and the highest coverage score.

D. Physical Robot Untangling Setup

Physical experiments are conducted on a single 3 m, white, braided USB-A to micro-USB cable, which is added to the workspace.

We evaluate TUSK in untangling performance on the following 3 levels of difficulty (Figure 6), where all knots are upward of 10 cm in diameter, and compare performance to SGTM 2.0 [31]:

- 1) **Tier C1:** A cable consisting of an overhand, figure 8, or overhand honda knot. The full cable configuration has ≤ 6 crossings.
- 2) **Tier C2:** A cable consisting of a bowline, linked overhand, or figure 8 honda knot. The full cable configuration has ≥ 6 and < 10 crossings.
- 3) **Tier C3:** A cable consisting of 2 knots (one of a knot class from Tier C2 and one of a knot class from Tier C1). The full cable configuration has ≥ 10 and < 15 crossings.

Similar to Shivakumar et al. [31], we use a 15-minute timeout on each rollout. We report metrics including success rate for untangling 1 and 2 knots, as well as the time to do so. We also report the success rate for termination, as well as the time required to do so, as a fraction of the number of rollouts that succeeded in fully untangling the cable.

VII. RESULTS

A. TUSK

As summarized in Table I, TUSK outperforms SGTM 2.0, TUSK (-LT), and TUSK (-CC) on categories 1 and 2. SGTM 2.0 outperforms TUSK in tier A2. This is because the Mask R-CNN is trained on dense overhand and figure 8 knots. While other knots in tier A2 are out of distribution, they visually resemble the overhand and figure 8 knots. The network is, therefore, able to still detect them as knots.

Failure Modes

- (A) The system fails to detect a knot that is present—a false negative.
- (B) The system detects a knot where there is no knot present—a false positive.
- (C) The tracer retraces previously traced regions of cable.
- (D) The crossing classification and correction schemes fail to infer the correct cable topology.
- (E) The knot detection algorithm does not fully isolate the knot, also getting surrounding trivial loops.

TABLE II: TUSK and Physical Robot Experiments (90 total trials)

	Tier C1		Tier C2		Tier C3	
	SGTM 2.0	TUSK	SGTM 2.0	TUSK	SGTM 2.0	TUSK
Knot 1 Success Rate	11/15	12/15	6/15	11/15	9/15	14/15
Knot 2 Success Rate	-	-	-	-	2/15	6/15
Verification Rate	11/11	8/12	6/6	6/11	1/2	2/6
Avg. Knot 1 Time (min)	1.09 ± 0.12	2.11 ± 0.25	3.45 ± 0.74	3.88 ± 1.09	1.84 ± 0.38	2.00 ± 0.42
Avg. Knot 2 Time (min)	-	-	-	-	3.11 ± 1.18	7.45 ± 1.55
Avg. Verif. Time (min)	5.71 ± 0.88	6.13 ± 1.44	6.35 ± 1.81	10.10 ± 0.67	5.38	9.58 ± 1.48
Failures	(7) 4	(1) 2, (2) 1	(1) 3, (5) 6	(2) 2, (4) 1, (5) 1	(1) 3, (2) 3, (5) 3, (6) 2, (7) 2	(1) 2, (2) 3, (3) 1, (6) 3

TABLE III: Multi-Cable Tracing Results

	Analytic	Learned
Tier B1	3/30	27/30
Tier B2	2/30	23/30
Tier B3	1/30	23/30
Failures	(I) 3, (II) 45, (III) 36	(I) 14, (II) 1, (III) 2

- (F) The trace skips a section of the true cable path.
- (G) The trace is incorrect in regions containing a series of close parallel crossings.
- (H) The tracer takes an incorrect turn, jumping to another cable segment.

For SGTM 2.0, the most common failure modes are (A) and (B), where it misses knots or incorrectly identifies knots when they are out of distribution. For TUSK (-LT), the most common failure modes are (F), (G), and (H). All 3 failures are trace-related and result in knots going undetected or being incorrectly detected. For TUSK (-CC), the most common failure modes are (B) and (E). This is because TUSK (-CC) is unable to distinguish between trivial loops and knots without the crossing cancellation scheme. By the same token, TUSK (-CC) is also unable to fully isolate a knot from surrounding trivial loops. For TUSK, the most common failure mode is (B). However, this is a derivative of failure mode (D), which is present in TUSK (-LT), TUSK (-CC), and TUSK. Crossing classification is a common failure mode across all systems and is a bottleneck for accurate knot detection. In line with this observation, we hope to dig deeper into accurate crossing classification in future work.

B. Tracing through Multi-Cable Settings

Table III shows that the learned tracer significantly outperforms the baseline analytic tracer on all 3 tiers of difficulty with a total of 81% success across the tiers.

Failure Modes:

- (I) Misstep in the trace, i.e. the trace did not reach any adapter.
- (II) The trace reaches the wrong adapter.
- (III) The trace reaches the correct adapter but is an incorrect trace.

The most common failure mode for the learned tracer, especially in Tier B3, is (I). One reason for such failures is the presence of multiple twists along the cable path (particularly in Tier B3 setups, which contain more complex inter-cable knot configurations). The tracer is also prone to deviating from the correct path on encountering parallel cable segments. In Tier B2, we observe two instances of failure mode (III), where the

trace was almost entirely correct in that it reached the correct adapter but skipped a section of the cable.

The most common failure modes across all tiers for the analytic tracer are (II) and (III). The analytic tracer particularly struggles in regions of close parallel cable segments and twists. As a result of the scoring metric, 87 of the 90 paths that we test reach an adapter; however, 45/90 paths did not reach the correct adapter. Even for traces that reach the correct adapter, the trace is incorrect, jumping to other cables and skipping sections of the true cable path.

C. Physical Robot Untangling

Results in Table II show that our TUSK-based untangling system (29/45) outperforms SGTM 2.0 (19/45) in untangling success rate across 3 tiers of difficulty. SGTM 2.0 is, however, faster than TUSK in each of the 3 tiers. This is due to the fact that TUSK requires a full trace of the cable. TUSK also requires the full cable to be in view in order to claim termination, which is difficult to achieve as the cable is $3 \times$ as long as the width of the workspace. Because the cable falls in varying complex configurations, many of which leave the visible workspace, the untangling algorithm performs cable reveal moves before detecting knots. This increases the time needed to untangle and verify that the cable is untangled, causing some runs to time out before verification.

On the other hand, SGTM 2.0 has false termination as its main failure mode because it does not account for the cable exiting the workspace. This is beneficial for speed because the system terminates as early as possible. However, the system fails when an off-workspace knot remains and goes undetected. This allows rollouts to end quickly, even if the cable is not untangled.

Failure Modes:

- (1) Incorrect actions create a complex knot.
- (2) The system misses a grasp on tight knots.
- (3) The cable falls off the workspace.
- (4) The cable drapes on the robot, creating an irrecoverable configuration.
- (5) False termination.
- (6) Manipulation failure.
- (7) Timeout.

The main failure modes in TUSK are (1), (2), and (6). Due to incorrect cable topology estimates, failure mode (1) occurs: a bad action causes the cable to fall into complex, irrecoverable states. Additionally, due to the limitations of the cage-pinch dilation and endpoint separation moves, knots sometimes get tighter during the process of untangling. While

the perception system is still able to perceive the knot and select correct grasp points, the robot grippers bump the tight knot, moving the entire knot and causing missed grasps (2). Lastly, we experience manipulation failures while attempting some grasps as the YuMi has a conservative controller (6). We hope to resolve these hardware issues in future work.

The main failure modes in SGTM 2.0 are (5) and (7). Perception experiments indicate that SGTM 2.0 has both false positives and false negatives for cable configurations that are out of distribution. (5) occurs when out-of-distribution knots go undetected. (7) occurs when trivial loops are identified as knots, preventing the algorithm from terminating.

VIII. LIMITATIONS AND FUTURE WORK

This approach has notable limitations: The robot system executing TUSK still depends on a depth camera. Future work will address this and aim to remove depth for the 1D deformable grasping task. TUSK is also dependent on a mono-color workspace. Future work will investigate generalizing TUSK to function independent of backgrounds, allowing the system to work in a non-solid, multi-color workspace that imitates home environments. Additionally, in real world scenarios, cables vary in color and thickness, so we will also pursue making TUSK invariant to cable appearance. Lastly, on the manipulation side, the untangling system struggles to grasp tight loops. Future work will explore servoing methods to improve grasping reliability in tight regions.

IX. CONCLUSION

This work presents TUSK, a perception pipeline that iteratively traces and determines the topology of semi-planar cable configurations, detects knots given the cable state, and detects graspable points for untangling the knots. Experiments show that TUSK can successfully trace a single cable in a multi-cable setting with 81% accuracy, significantly outperforming an analytic baseline. TUSK is also able to detect knots with 77% accuracy. Lastly, when TUSK is applied to a robot untangling problem, the system is able to achieve 64% success in untangling.

ACKNOWLEDGEMENT

This research was performed at the AUTOLAB at UC Berkeley in affiliation with the Berkeley AI Research (BAIR) Lab, the CITRIS “People and Robots” (CPAR) Initiative, and the RealTime Intelligent Secure Execution (RISE) Lab. The authors were supported in part by donations from Toyota Research Institute and by equipment grants from PhotoNeo, and Nvidia.

REFERENCES

- [1] Yahav Avigal, Lars Berscheid, Tamim Asfour, Torsten Kröger, and Ken Goldberg. Speedfolding: Learning efficient bimanual folding of garments, 2022. URL <https://arxiv.org/abs/2208.10552>.
- [2] Lawrence Yunliang Chen, Baiyu Shi, Daniel Seita, Richard Cheng, Thomas Kollar, David Held, and Ken Goldberg. Autobag: Learning to open plastic bags and insert objects, 2022. URL <https://arxiv.org/abs/2210.17217>.
- [3] Cheng Chi, Benjamin Burchfiel, Eric Cousineau, Siyuan Feng, and Shuran Song. Iterative residual policy for goal-conditioned dynamic manipulation of deformable objects. In *Proceedings of Robotics: Science and Systems (RSS)*, 2022.
- [4] Blender Online Community. *Blender - a 3D modelling and rendering package*. Blender Foundation, Stichting Blender Foundation, Amsterdam, 2018. URL <http://www.blender.org>.
- [5] Peter R Florence, Lucas Manuelli, and Russ Tedrake. Dense object nets: Learning dense visual object descriptors by and for robotic manipulation. In *Conf. on Robot Learning (CoRL)*, 2018.
- [6] Aditya Ganapathi, Priya Sundaresan, Brijen Thananjeyan, Ashwin Balakrishna, Daniel Seita, Jennifer Grannen, Minho Hwang, Ryan Hoque, Joseph E Gonzalez, Nawid Jamali, et al. Learning to smooth and fold real fabric using dense object descriptors trained on synthetic color images. In *Proc. IEEE Int. Conf. Robotics and Automation (ICRA)*, 2021.
- [7] Jennifer Grannen, Priya Sundaresan, Brijen Thananjeyan, Jeffrey Ichnowski, Ashwin Balakrishna, Minho Hwang, Vainavi Viswanath, Michael Laskey, Joseph E Gonzalez, and Ken Goldberg. Untangling dense knots by learning task-relevant keypoints. *Conference on Robot Learning*, 2020.
- [8] Ryan Hoque, Daniel Seita, Ashwin Balakrishna, Aditya Ganapathi, Ajay Kumar Tanwani, Nawid Jamali, Katsu Yamane, Soshi Iba, and Ken Goldberg. Visuospatial foresight for multi-step, multi-task fabric manipulation. In *Proc. Robotics: Science and Systems (RSS)*, 2020.
- [9] Ryan Hoque, Kaushik Shivakumar, Shrey Aeron, Gabriel Deza, Aditya Ganapathi, Adrian Wong, Johnny Lee, Andy Zeng, Vincent Vanhoucke, and Ken Goldberg. Learning to fold real garments with one arm: A case study in cloud-based robotics research. In *2022 IEEE/RSJ International Conference on Intelligent Robots and Systems (IROS)*, pages 251–257, 2022. doi: 10.1109/IROS47612.2022.9981253.
- [10] Xuzhao Huang, Dayuan Chen, Yuhao Guo, Xin Jiang, and Yunhui Liu. Untangling multiple deformable linear objects in unknown quantities with complex backgrounds. *IEEE Transactions on Automation Science and Engineering*, pages 1–13, 2023. doi: 10.1109/TASE.2023.3233949.
- [11] Pavel Iakubovskii. Segmentation models pytorch. https://github.com/qubvel/segmentation_models.pytorch, 2019.
- [12] Russell C. Jackson, Rick Yuan, Der-Lin Chow, Wyatt S. Newman, and M. Cenk Çavuşoğlu. Real-time visual tracking of dynamic surgical suture threads. *IEEE Transactions on Automation Science and Engineering*, 15(3):1078–1090, 2018. doi: 10.1109/TASE.2017.2726689.
- [13] Azarakhsh Keipour, Maryam Bandari, and Stefan Schaal. Deformable one-dimensional object detection for routing and manipulation. *CoRR*, abs/2201.06775, 2022. URL <https://arxiv.org/abs/2201.06775>.
- [14] Diederik P Kingma and Jimmy Ba. Adam: A method for stochastic optimization. In *International Conference on Learning Representations*, 2015.
- [15] Thomas Kollar, Michael Laskey, Kevin Stone, Brijen Thananjeyan, and Mark Tjersland. Simnet: Enabling robust unknown object manipulation from pure synthetic data via stereo. In *Conference on Robot Learning*, pages 938–948. PMLR, 2022.
- [16] Robert Lee, Daniel Ward, Akansel Cosgun, Vibhavari Dasagi, Peter Corke, and Jurgen Leitner. Learning arbitrary-goal fabric folding with one hour of real robot experience. In *Conf. on Robot Learning (CoRL)*, 2020.
- [17] Xingyu Lin, Yufei Wang, Zixuan Huang, and David Held. Learning visible connectivity dynamics for cloth smoothing. In *Conference on Robot Learning*, pages 256–266. PMLR, 2022.
- [18] Wen Hao Lui and Ashutosh Saxena. Tangled: Learning to untangle ropes with rgb-d perception. In *2013 IEEE/RSJ Int. Conf. on Intelligent Robots and Systems*, 2013.
- [19] Wen Hao Lui and Ashutosh Saxena. Tangled: Learning to untangle ropes with RGB-D perception. In *2013 IEEE/RSJ Int. Conf. on Intelligent Robots and Systems*, pages 837–844. IEEE, 2013.
- [20] Jan Matas, Stephen James, and Andrew J Davison. Sim-to-real reinforcement learning for deformable object manipulation. In *Conf. on Robot Learning (CoRL)*, 2018.
- [21] Hermann Mayer, Faustino Gomez, Daan Wierstra, Istvan Nagy, Alois Knoll, and Jürgen Schmidhuber. A system for robotic heart surgery that learns to tie knots using recurrent neural networks. *Advanced Robotics*, 22(13-14):1521–1537, 2008.
- [22] Dale McConachie, Thomas Power, Peter Mitrano, and Dmitry Berenson. Learning when to trust a dynamics model for planning in reduced state spaces. *CoRR*, abs/2001.11051, 2020. URL <https://arxiv.org/abs/2001.11051>.
- [23] Ashvin Nair, Dian Chen, Pulkit Agrawal, Phillip Isola, Pieter Abbeel, Jitendra Malik, and Sergey Levine. Combining self-supervised learning and imitation for vision-based rope manipulation. *CoRR*, abs/1703.02018, 2017. URL <http://arxiv.org/abs/1703.02018>.
- [24] Nicolas Padoy and Gregory Hager. Deformable tracking of textured curvilinear objects. In *Proceedings of the British Machine Vision*

Conference, pages 5.1–5.11. BMVA Press, 2012. ISBN 1-901725-46-4. doi: <http://dx.doi.org/10.5244/C.26.5>.

[25] Paritosh Parmar. Use of computer vision to detect tangles in tangled objects. In *2013 IEEE Second International Conference on Image Information Processing (ICIIP-2013)*. IEEE, dec 2013. doi: 10.1109/iciip.2013.6707551.

[26] Kurt Reidemeister. *Knot theory*. BCS Associates, 1983.

[27] Jose Sanchez, Juan-Antonio Corrales, Belhassen-Chedli Bouzgarrou, and Youcef Mezouar. Robotic manipulation and sensing of deformable objects in domestic and industrial applications: a survey. *The International Journal of Robotics Research*, 37(7):688–716, 2018.

[28] John Schulman, Alex Lee, Jonathan Ho, and Pieter Abbeel. Tracking deformable objects with point clouds. In *2013 IEEE International Conference on Robotics and Automation*, pages 1130–1137, 2013. doi: 10.1109/ICRA.2013.6630714.

[29] Daniel Seita, Aditya Ganapathi, Ryan Hoque, Minho Hwang, Edward Cen, Ajay Kumar Tanwani, Ashwin Balakrishna, Brijen Thananjeyan, Jeffrey Ichnowski, Nawid Jamali, et al. Deep imitation learning of sequential fabric smoothing from an algorithmic supervisor. In *Proc. IEEE/RSJ Int. Conf. on Intelligent Robots and Systems (IROS)*, 2020.

[30] Daniel Seita, Pete Florence, Jonathan Tompson, Erwin Coumans, Vikas Sindhwani, Ken Goldberg, and Andy Zeng. Learning to rearrange deformable cables, fabrics, and bags with goal-conditioned transporter networks. In *Proc. IEEE Int. Conf. Robotics and Automation (ICRA)*, 2021.

[31] Kaushik Shivakumar, Vainavi Viswanath, Anrui Gu, Yahav Avigal, Justin Kerr, Jeffrey Ichnowski, Richard Cheng, Thomas Kollar, and Ken Goldberg. Sgtn 2.0: Autonomously untangling long cables using interactive perception. *arXiv preprint arXiv:2209.13706*, 2022.

[32] Yu Song, Kang Yang, Xin Jiang, and Yunhui Liu. Vision based topological state recognition for deformable linear object untangling conducted in unknown background. In *2019 IEEE International Conference on Robotics and Biomimetics (ROBIO)*, pages 790–795, 2019. doi: 10.1109/ROBIO49542.2019.8961652.

[33] Priya Sundaresan, Jennifer Grannen, Brijen Thananjeyan, Ashwin Balakrishna, Michael Laskey, Kevin Stone, Joseph E Gonzalez, and Ken Goldberg. Learning rope manipulation policies using dense object descriptors trained on synthetic depth data. In *Proc. IEEE Int. Conf. Robotics and Automation (ICRA)*, 2020.

[34] Priya Sundaresan, Jennifer Grannen, Brijen Thananjeyan, Ashwin Balakrishna, Jeffrey Ichnowski, Ellen Novoseller, Minho Hwang, Michael Laskey, Joseph E Gonzalez, and Ken Goldberg. Untangling dense non-planar knots by learning manipulation features and recovery policies. *Proc. Robotics: Science and Systems (RSS)*, 2021.

[35] Te Tang and Masayoshi Tomizuka. Track deformable objects from point clouds with structure preserved registration. *The International Journal of Robotics Research*, 41(6):599–614, 2022. doi: 10.1177/0278364919841431. URL <https://doi.org/10.1177/0278364919841431>.

[36] Brijen Thananjeyan, Justin Kerr, Huang Huang, Joseph E. Gonzalez, and Ken Goldberg. All you need is luv: Unsupervised collection of labeled images using invisible uv fluorescent indicators, 2022. URL <https://arxiv.org/abs/2203.04566>.

[37] Jur Van Den Berg, Stephen Miller, Daniel Duckworth, Humphrey Hu, Andrew Wan, Xiao-Yu Fu, Ken Goldberg, and Pieter Abbeel. Superhuman performance of surgical tasks by robots using iterative learning from human-guided demonstrations. In *2010 IEEE International Conference on Robotics and Automation*, pages 2074–2081. IEEE, 2010.

[38] Vainavi Viswanath, Jennifer Grannen, Priya Sundaresan, Brijen Thananjeyan, Ashwin Balakrishna, Ellen Novoseller, Jeffrey Ichnowski, Michael Laskey, Joseph E Gonzalez, and Ken Goldberg. Disentangling dense multi-cable knots. *Proc. IEEE/RSJ Int. Conf. on Intelligent Robots and Systems (IROS)*, 2021.

[39] Vainavi Viswanath, Kaushik Shivakumar, Justin Kerr, Brijen Thananjeyan, Ellen Novoseller, Jeffrey Ichnowski, Alejandro Escontrela, Michael Laskey, Joseph E Gonzalez, and Ken Goldberg. Autonomously untangling long cables. *Robotics: Science and Systems (RSS)*, 2022.

[40] Angelina Wang, Thanard Kurutach, Kara Liu, Pieter Abbeel, and Aviv Tamar. Learning robotic manipulation through visual planning and acting. *Robotics: Science and Systems (RSS)*, 2019.

[41] Thomas Weng, Sujay Man Bajracharya, Yufei Wang, Khush Agrawal, and David Held. Fabricflownet: Bimanual cloth manipulation with a flow-based policy. In *Conference on Robot Learning*, pages 192–202. PMLR, 2022.

[42] Yilin Wu, Wilson Yan, Thanard Kurutach, Lerrel Pinto, and Pieter Abbeel. Learning to manipulate deformable objects without demonstrations. *arXiv preprint arXiv:1910.13439*, 2019.

[43] Yuji Yamakawa, Akio Namiki, Masatoshi Ishikawa, and Makoto Shimojo. One-handed knotting of a flexible rope with a high-speed multifingered hand having tactile sensors. In *2007 IEEE/RSJ Int. Conf. on Intelligent Robots and Systems*, pages 703–708. IEEE, 2007.

[44] Wilson Yan, Ashwin Vangipuram, Pieter Abbeel, and Lerrel Pinto. Learning predictive representations for deformable objects using contrastive estimation. In *Conf. on Robot Learning (CoRL)*, 2020.